LANGMUIR

Article

pubs.acs.org/Langmuir

Selective Adsorption and Separation through Molecular Filtration by Hyperbranched Poly(ether amine)/Carbon Nanotube Ultrathin Membranes

Yuannan Zhang, Xiaodong Ma, Hongjie Xu, Zixing Shi, Jie Yin, and Xuesong Jiang*

State Key Laboratory for Metal Matrix Composite Materials, School of Chemistry & Chemical Engineering, Shanghai Jiao Tong University, Shanghai 200240, People's Republic of China

Supporting Information

ABSTRACT: In response to the increasing public awareness of serious dye-contained wastewater contamination, we herein fabricated a novel anthracene-containing hyperbranched poly(ether amine) (hPEA-AN)/carbon nanotube (CNT) ultrathin membrane (UTM), which combined both the merits of the conventional dye adsorption strategy and membrane filtration process, to implement efficient selective adsorption of dye molecules and also the separation of dye mixtures by molecular filtration. Taking advantage of the $\pi-\pi$ stacking interactions between anthracene and CNT sidewalls and hydrophobic interactions, CNTs were coated tightly with hPEA-AN to form the hPEA-AN@CNT complex, which can be well-dispersed very stably in water. The formation of the hPEA-AN@CNT complex was confirmed using X-ray photoelectron spectroscopy, Raman spectra, fluorescence spectra, and thermogravimetric analysis. Meanwhile, a simple filtration process was applied to prepare hPEA-AN@CNT UTMs with a thickness of 1.5 μm, which can be further cross-linked through photodimerization of anthracene moieties. The UTMs represented selective adsorption behaviors toward hydrophilic dyes even with similar backbones and the same charge states, namely, they showed high adsorption capacities (Q_{eq}) toward eosin B, erythrosin B (ETB), 4′,5′-dibromofluorescein, and Evans blue (EVB) dyes up to 300 μmol/g while showing low adsorption capacities toward calcein (Cal), methyl red, and Ponceau S dyes. On the basis of this unique selective adsorption, molecular filtration was then realized toward mixed ETB/Cal and EVB/Cal dyes, with a separation efficiency of up to 100% and regeneration without an obvious efficiency decrease.

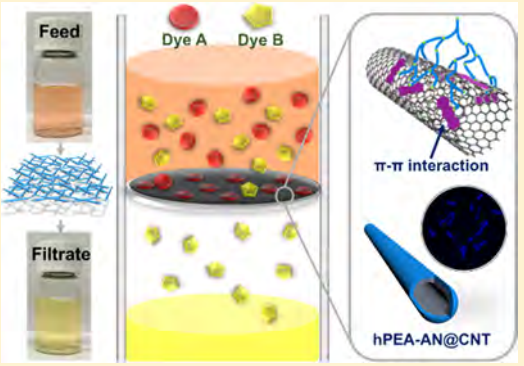

INTRODUCTION

The global occurrence of clean water resources being threatened by colored micropollutants has raised widespread concerns.[1] Colored dyes were the first recognized contaminants in wastewater[2] and are widely used in industries such as textile printing, paper, and plastics,[3] resulting in increased side effects on aquatic ecosystems and on human health owing to their toxicity and nonbiodegradability.[4] As a consequence, an efficient separation technology for dye removal from wastewater is the prompt solution in demand. However, dye-containing wastewater treatment is a chronic problem owing to the recalcitrance of organic dyes, stability to light and heat, and the resistance to aerobic digestion.[5,6]

So far, among the numerous dye removal techniques, such as chemical precipitation, photocatalytic and photolytic biodegradation, and advanced oxidative degradation,[7−11] adsorption has been a better option that brings one of the best outcomes in removing different types of colored molecules and with a relatively low cost,[12] where common adsorbents possess porous structures to enlarge the exposed surface area for stronger interactions.[13,14] Most widely used commercial adsorbent materials such as activated carbons exhibit excellent adsorption ability but poor removal of many relatively hydrophilic micropollutants,[15] low selectivity for similar molecules, and concurrently high costs of regeneration without complete restoration.[14] Various hydrogels, nanoparticles, and functionalized fibrous materials are effective for static adsorption,[16−19] whereas selectivity is a particularly important factor for adsorbents in the wastewater treatment industry, where dye mixtures are always a complex component and thus are difficult to separate and reuse. Adsorbents with selective adsorption properties enable the separation of similar guest molecules, and researchers have been engaged in many valuable works such as constructing selective adsorption materials. Broer, Schenning, and co-workers prepared efficient and selective porous-nanostructured adsorbents based on a smectic liquid-crystal polymer, which possessed confined pore dimensions allowing size-selective adsorption of hydrophilic dyes.[20] Molina and co-workers have reported a stimuli-sensitive ureasil−polyether-siloxane hybrid matrix that could easily and rapidly separate anionic dyes from a mixture containing anionic and cationic dyes.[21] Wan and co-workers studied charge-selective separation

Received: October 10, 2016
Revised: November 13, 2016
Published: November 14, 2016

DOI: 10.1021/acs.langmuir.6b03689
Langmuir XXXX, XXX, XXX−XXX

Scheme 1. Schematic of the Preparation of hPEA-AN@CNT UTM[a]

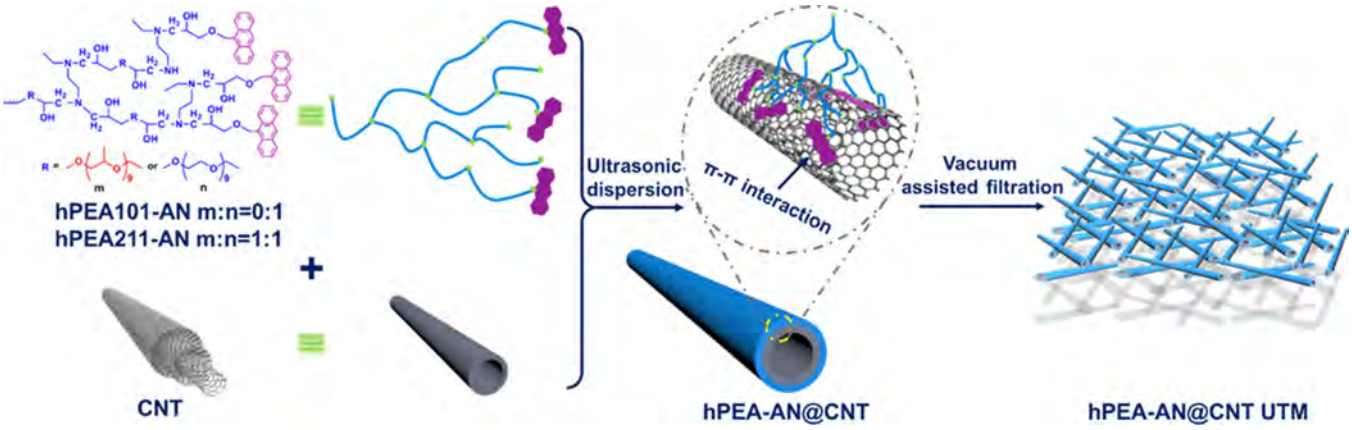

[a]The mixture of hPEA-AN and CNT first formed the hPEA-AN@CNT complex through $\pi-\pi$ interactions between AN and CNT sidewalls under ultrasonic dispersion; then, dispersion of the complex was followed by simple vacuum-assisted filtration to fabricate hPEA-AN@CNT UTMs.

and recovery of organic ionic dyes by polymeric micelles, which extracted an anionic dye from cationic contaminants and transferred them from an aqueous phase to an apolar oil phase.[22] The selective adsorption mechanisms of most of the reported studies generally cover size selectivity and charge selectivity for guest molecules with different sizes or charge states.[23−27] To the best of our knowledge, however, studies on selective adsorption of dyes with similar sizes, similar backbones, and the same charge states are limited and remain challenging.

Recently, our group has developed a novel multifunctional hyperbranched poly(ether amine) (hPEA) and found that the hPEA-based hydrogels and their interpenetrating networks exhibit a unique selective adsorption and separation of dye molecules with similar backbones and the same charge states that is dependent on hydrophilic−hydrophobic interactions.[28−32] At the same time, the PEA nanofiber membrane produced by electrospinning can be used for the selective adsorption and separation of dyes through membrane filtration.[33] Traditional membrane filtration including ultrafiltration and nanofiltration is an attractive advanced water treatment technology because of its well-known size-exclusion effect for solutes that are larger than the pore size of the membranes.[34−37] The combination of selective adsorption and membrane filtration strategies opens a novel but vital window for developing efficient dye-removal technologies. Besides size selectivity, the membranes acquired an additional adsorption function,[38−41] which promotes the improvement of adsorption techniques.

Hence, we here progressively pioneer a new approach that combines the excellent selective adsorption behavior of hPEA and the advantages of membrane filtration, avoiding the cumbersome preparation process, expecting to afford the aforementioned adsorption filtrated membranes via simple green techniques. As is well-known, fibrous carbon nanotubes (CNTs) have demonstrated their potential utilization in many fields because of their mechanical, thermal, and electrical properties,[42,43] particularly in building high-performance fibers applied in the upcoming application realm of water filtration.[44,45] Studies on CNT composite clay[46,47] and film for water−oil separation[48−50] and heavy metal removal[51] have been carried out, whereas the task of removal of dyes still requires in-depth research because of the shortcomings of complex tedious preparation processes[52,53] and low selectivity.[54] Nevertheless, a CNT is an ideal vehicle in our designed adsorption filter system. In this study, the CNT was first decorated with anthracene-containing hyperbranched poly(ether amine) (hPEA-AN) to form the fibrous hPEA-AN@CNT complex in water through noncovalent $\pi-\pi$ stacking and hydrophobic interactions between hPEA-AN and CNT sidewalls; then, ultrathin membranes (UTMs) of hPEA-AN@CNTs were fabricated using a simple vacuum-assisted filtration process thanks to the fibrous structure with a high aspect ratio of a hPEA-AN@CNT complex with good water dispersion (Scheme 1). The high specific surface area and high water penetrability of the obtained three-dimensional fibrous hPEA-AN@CNT nanoscale network ensures maximized conduction between guest dye molecules and host UTMs for the utilization of molecular adsorption filtration, leading to the feasibility of uptake of different dye molecules from wastewater solutions by hPEA-AN@CNT UTMs. The strong mechanical strength of CNT fibers is an advantage, which makes the UTMs strong and stable for reuse. The resulting UTMs of hPEA-AN@CNTs not only exhibit efficient selective adsorption and remove hydrophilic dye from wastewater but also show high separation efficiency of dye molecules even with similar backbones and the same charge states through molecular filtration.

RESULTS AND DISCUSSION

Fabrication and Characterization of hPEA-AN@CNT UTMs. Amphiphilic hPEA is composed of short polyether chains in the backbone and a large amount of secondary amino groups in the periphery. Anthracene moieties were introduced into the periphery of hPEA to obtain anthracene-ending hPEA (hPEA-AN). By adjusting the components of polyether chains poly(ethylene oxide) (PEO) and polyphenylene oxide (PPO), hPEA-AN with different hydrophilicities (hPEA101-AN and hPEA211-AN) could be acquired according to our previous work.[55] The whole strategy for preparing hPEA-AN/CNT UTMs is illustrated in Scheme 1, where the mixture of hPEA-AN and CNT first underwent ultrasonic dispersion in water to afford hPEA-AN-coated CNT fibers (hPEA-AN), which further formed uniform UTMs by the foolproof vacuum-assisted filtration process.

Because of the strong $\pi-\pi$ stacking and hydrophobic interactions between the anthracene moieties and sidewalls of

DOI: 10.1021/acs.langmuir.6b03689
Langmuir XXXX, XXX, XXX−XXX

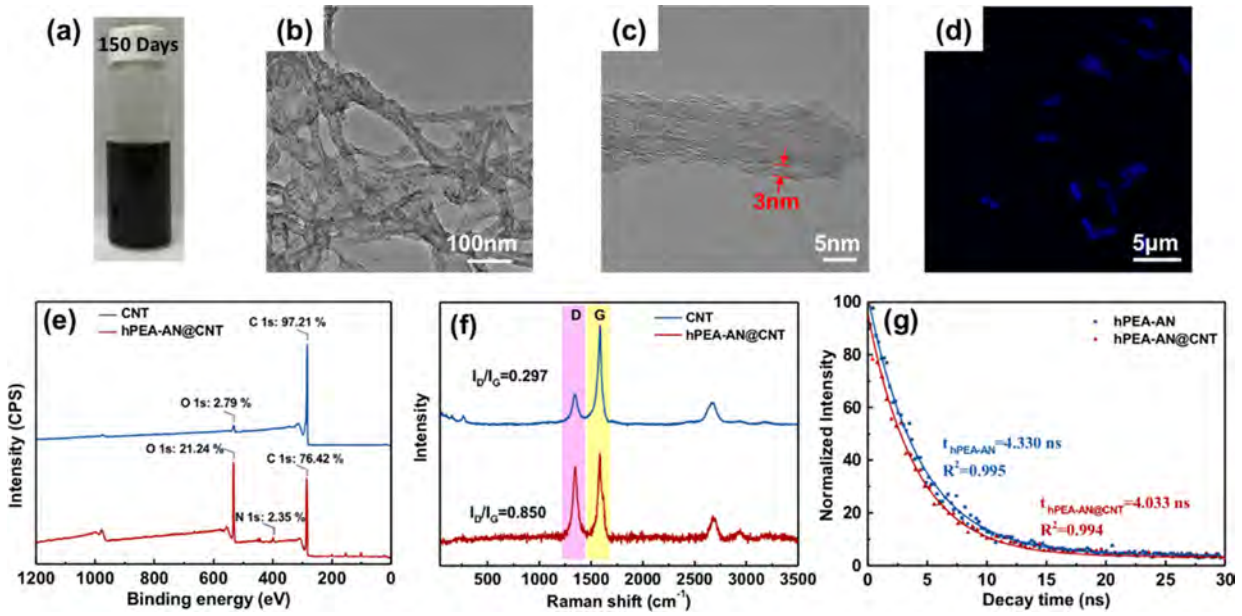

Figure 1. Characterization of hPEA211-AN@CNT: (a) dispersion of hPEA-AN@CNTs for 150 days; (b,c) TEM images of hPEA-AN-coated CNTs; (d) LSCM image of hPEA-AN@CNTs; (e) XPS spectra with atomic concentration (%); (f) Raman spectra; (g) effect of hPEA-AN coating on fluorescence decay.

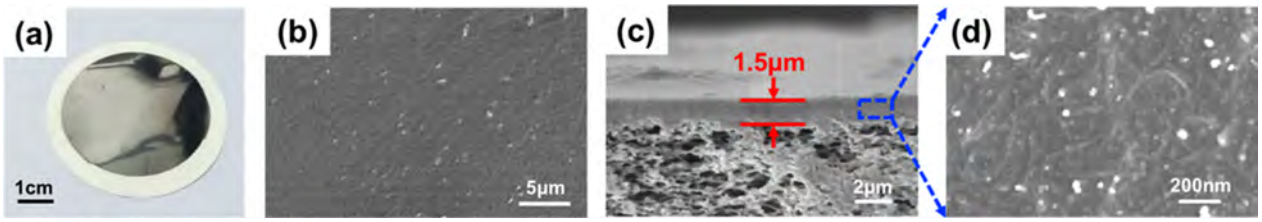

Figure 2. Characterization of hPEA211-AN@CNT UTMs: (a) photograph of the UTM; (b–d) SEM images of surface (b) and section (c,d) of the UTM.

the CNT,[56−59] the CNT was well-coated with hPEA-AN to form the hPEA-AN@CNT complex by mixing hPEA-AN and CNTs in an aqueous solution. As shown in Figure 1a, the resultant hPEA-AN@CNT complex was dispersed very stably in an aqueous solution over a long period of more than 150 days, indicating the strong interactions between hPEA-AN and CNT. On the contrary, the hydrophobic CNTs could not be dispersed alone in water in the absence of hPEA-AN (Figure S1a). Even with the help of hPEA without AN moieties, the CNTs could not be dispersed stably in water and settled after 10 days (Figure S1b). This indicated that the $\pi-\pi$ stacking interaction between AN and CNTs is very important in the formation of the stable hPEA-AN@CNT complex in water. It is interesting that the stimuli-responsive performance of a hPEA-AN layer allows for the controlled dispersion of hPEA-AN@CNT in response to temperature.[60] After heating at >80 °C, hPEA-AN@CNTs began to aggregate and then precipitated from an aqueous solution at the bottom (Figure S1c). It should be noted that this process is reversible. After cooling to room temperature, the precipitated hPEA-AN@CNTs can be dispersed in water again. This reversible dispersion behavior also supported the formation of the stable hPEA-AN@CNT complex in water.

We then conducted a series of analysis experiments to investigate the resultant hPEA-AN@CNT in detail (Figure 1), and all measurements were taken with hPEA211-AN@CNT as an example. The hPEA-AN layer coated on the CNT was observed using transmission electron microscopy (TEM), and the thickness is around 3 nm in comparison with that of the pristine CNTs (Figures 1b,c and S1d). To confirm the completeness and uniformity of the coating layer, laser scanning confocal microscopy (LSCM) was carried out, and the fluorescence image revealed that hPEA-AN@CNT exhibited strong blue fluorescence (Figure 1d) thanks to the emission of anthracene moieties of hPEA-AN layers coated on the surface of CNTs. The resultant hPEA-AN@CNT aqueous solution presented the characteristic ultraviolet (UV)−vis and fluorescence spectra peaks of anthracene (Figure S2). In comparison with the pristine CNT, the lyophilized hPEA-AN@CNT powder withstood the X-ray photoelectron spectroscopy (XPS) test (Figure 1e), resulting in the appearance of a N 1s peak (atomic concentration of 2.35%), an increase in the atomic concentration of O (from 2.79 to 21.24%), and a decrease in the atomic concentration of C (from 97.21 to 76.42%), corresponding to the introduction of hPEA-AN. Meanwhile, on the basis of the weight loss of CNTs, hPEA-AN, and hPEA-AN@CNTs at 600 °C measured using a thermogravimetric analyzer (TGA), the hPEA-AN coating rate was calculated to be around 81% (Figure S3 and Table S1).

It is the existence of aromatic anthracene moieties that enable the $\pi-\pi$ interactions between hPEA-AN and the outer surface of CNTs. Raman spectra showed strong evidence for

DOI: 10.1021/acs.langmuir.6b03689
Langmuir XXXX, XXX, XXX−XXX

Scheme 2. Structures and Abbreviation of 12 Different Hydrophilic Dyes Belonging to Three Families

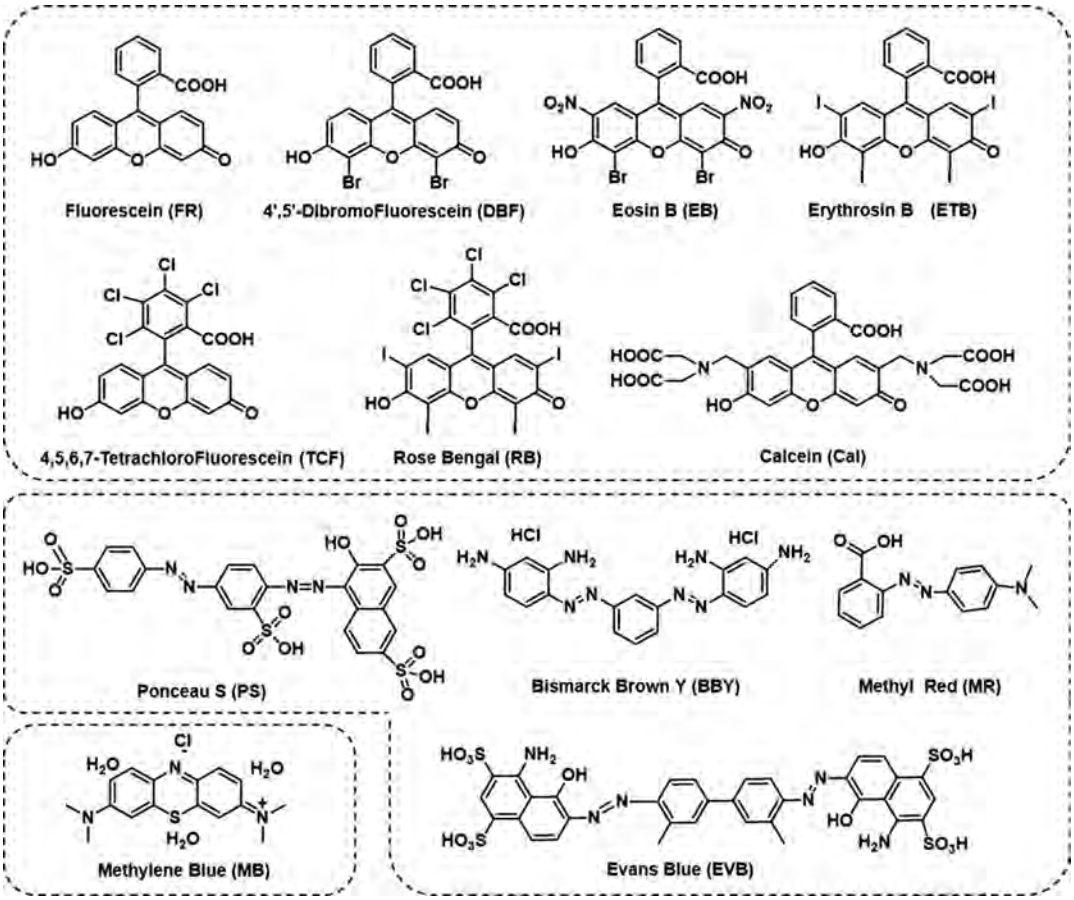

the transition from sp^2 to sp^3 hybridization of C atoms from graphite bonding to disordered bonding in the graphitic sidewalls of the CNTs[61] because the value of I_D/I_G significantly increased after hPEA-AN modification (Figure 1f). In addition, compared with hPEA-AN, hPEA-AN@CNTs in the aqueous solution presented a shorter lifetime of AN fluorescence (τ = 4.033 ns) according to fluorescence decay results (Figure 1g), which should be ascribed to the microenvironmental variation in the excited anthracene molecules brought by the CNTs leading to an additional dynamic quenching.[62] All of these data confirmed that the hPEA-AN layer was coated on CNTs to form the stable hPEA-AN@CNT complex.

With the improved dispersion of CNTs coated with hPEA-AN layers in water, UTMs could be fabricated using the vacuum-assisted sand core filtration process, and the diameter of the smooth UTMs obtained was 4.5 cm (Figure 2a). It is remarkable that the obtained hPEA211-AN@CNT UTMs possessed an immaculately reflective surface, which proved that the membrane structure was extremely uniform, demonstrating the excellent dispersion of hPEA-AN@CNTs from another point of view. To further observe the microstructure of the UTMs, scanning electron microscopy (SEM) was carried out to view the surface and cross-sectional morphologies (Figure 2b–d). The UTMs have a smooth and compact surface, as seen in the SEM image (Figure 2b), and the thickness of the cross section was around 1.5 μm (Figure 2c). The fibrous CNTs were apparent in the enlarged view (Figure 2d), whereas the head of a handful of hPEA-AN@CNTs in the matrix that was exposed in the low-temperature brittle fracture process might be attributed to brighter white points. At the same time, the component and the thickness of hPEA-AN@CNT UTMs were controllable by adjusting the synthesis and manufacturing technologies. UTMs with different hPEA components (hPEA101-AN and hPEA211-AN) could be obtained depending on the contents of PEO and PPO in the synthesis process, whereas UTMs with varied thicknesses could be prepared by controlling the concentration and volume of the dispersed solution added in the filtration process. hPEA101-AN@CNT UTMs with a thickness of 10 μm were prepared, which presented a reflective surface as well (Figure S4a), and the SEM images (Figure S4b–d) revealed surface and cross-sectional morphologies similar to those of the above-mentioned hPEA211-AN@CNT UTMs.

To make sure that the UTMs would be steady when undergoing the following batch adsorption tests and molecular filtration procedures and that neither hPEA-AN nor CNT molecules would be dissolved out of the membranes, cross-linking through anthracene photodimerization was carried out. The UTMs were illuminated under a 365 nm UV lamp for 30 min to make sure that most AN moieties in the coating layers were photodimerized and fixed on one CNT fiber; meanwhile, the AN moieties on the surface of each hPEA-AN@CNT fiber could undergo interfibrous dimerization to cross-link the entire membrane. The process for photocross-linking of anthracene in the hPEA-AN@CNT aqueous solution was traced using UV–vis spectra (Figure S5).

Selective Adsorption Behavior of Hydrophilic Dyes. The uptake of 12 hydrophilic dyes common in the textile and paper-making industry was tested; these dyes belong to three typical families (Scheme 2): fluorescein dye, azo dye, and

DOI: 10.1021/acs.langmuir.6b03689
Langmuir XXXX, XXX, XXX–XXX

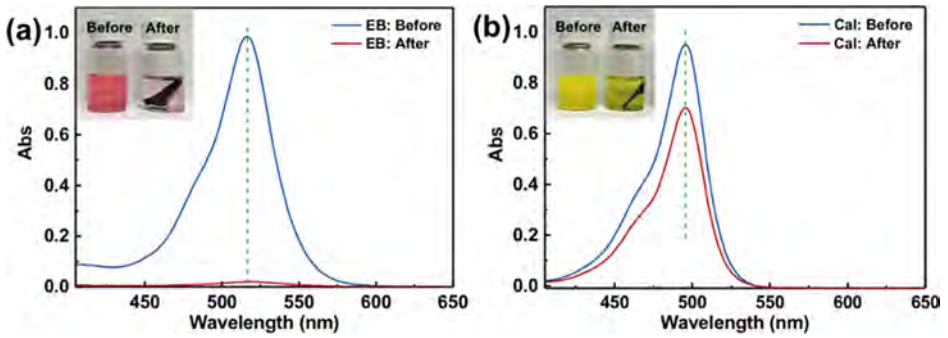

Figure 3. Selective adsorption behaviors toward EB and Cal dyes: UV−vis spectra of EB (a) and Cal (b) before and after batch adsorption by hPEA211-AN@CNT UTMs for 48 h. Insets are photographs of solutions of EB and Cal before and after adsorption.

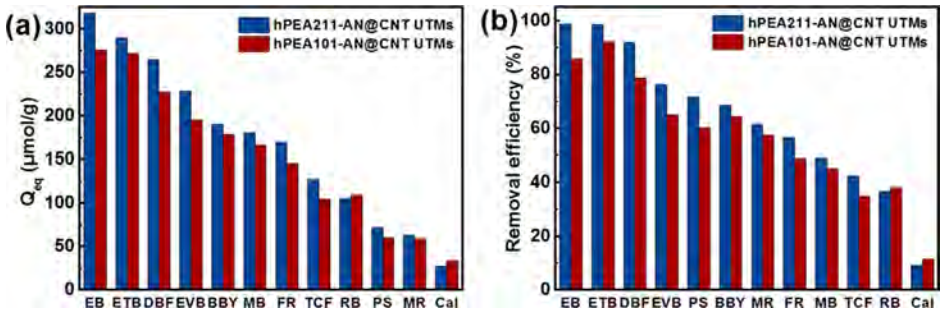

Figure 4. Batch adsorption capacities and removal efficiencies toward 12 hydrophilic dyes: (a) equilibrium adsorption capacities of hPEA-AN@CNT UTMs for the uptake of 12 different hydrophilic dyes in phosphate buffer and (b) percentage removal efficiency of each dye obtained by the batch adsorption of hPEA-AN@CNT UTMs at 25 °C (6 mL of dye solution with initial concentration of 300 μmol/L, adsorbent 5 mg, pH = 7.2, adsorption time 48 h).

phenothiazine dye. Four azo dyes, Ponceau S (PS), Bismarck brown Y (BBY), methyl red (MR), and Evans blue (EVB), were chosen because of their extremely broad use in printing and dyeing technology; they can break down in water over time to give rise to carcinogenic aromatic amines that are toxic and cannot be degraded naturally.[63] Methylene blue (MB), a cationic dye that represents phenothiazine dyes, is widely applied in biochemical tests, aquaculture, and tintage, whereas the overuse of the dye still causes a lot of environmental problems and needs to be dealt with.[39] Fluorescein dyes including fluorescein (FR), 4′,5′-dibromofluorescein (DBF), eosin B (EB), erythrosin B (ETB), 4,5,6,7-tetrachlorofluorescein, rose bengal, and calcein (Cal) were selected because of their same backbones and negatively charged states in aqueous solution, which is helpful for understanding the interaction between dyes and hPEA-AN@CNTs and the adsorption mechanism.

hPEA-AN@CNT UTMs possess a three-dimensional nanoscale network structure of coated nanotubes because of the specific filtrating preparation technology, which may make them good candidates in the adsorption of dyes from wastewater. Batch adsorption capabilities of hPEA-AN@CNT UTMs were measured by detecting the equilibrium uptake, which is regarded as a function of residual dye concentration after adsorption via UV−vis spectra. Toward different dyes, the adsorptive capacity of hPEA-AN@CNT UTMs varied a lot. For instance, hPEA211-AN@CNT UTMs showed the opposite adsorption behavior when adsorbing EB and Cal dyes (Figure 3). Almost all of the EB dye was adsorbed by the UTMs when reaching equilibrium according to the UV−vis spectra, which was also reflected by the obvious faded color after adsorption (Figure 3a and the inset image). In contrast to the remarkable uptake of the EB dye, hPEA-AN@CNT UTMs did not adsorb Cal in the dye solution that much: Cal remained in solution, and the color of the dye solution stayed almost unchanged (Figure 3b and the inset image). The preliminary results revealed that nearly 99% of the EB dye was taken by the hPEA-AN@CNT UTMs, whereas just about 25% of the Cal dye was adsorbed.

Furthermore, we probed the equilibrium adsorption capacity (Q_{eq}), one of the major parameters used to evaluate the adsorption capacity under the experimental conditions (see the Batch Adsorption of Twelve Hydrophilic Dyes section). To understand the selectivity obtained from both host materials and guest molecules, we compared the removal efficiency of hPEA-AN@CNT membranes in the 12 different hydrophilic guest dye molecules fabricated by two kinds of host molecules: relatively more hydrophobic hPEA211-AN and relatively hydrophilic hPEA101-AN. As shown in Figure 4a, hPEA211-AN@CNT UTMs (blue bars) showed high Q_{eq} toward several fluorescein and azo dyes such as EB and ETB up to 300 μmol/g, whereas for Cal, low Q_{eq} was found below 30 μmol/g. It is worth noting that the uptake of negatively charged Cal by hPEA-AN with positively charged amino groups was the lowest, indicating that the host hPEA211-AN@CNTs and guest dye molecules maintain electrostatic noninterference and electrostatic interactions were not the main acting force.

For dyes with more hydrophobic substituents, hPEA211-AN@CNT UTMs presented a stronger adsorption ability, suggesting that the hydrophobicity of the adsorbents may be crucial to the uptake of guest molecules. In the meantime, compared with that of the relatively hydrophilic hPEA101-AN@CNT UTMs (Figure 4a, red bars), the slightly higher Q_{eq} of hPEA211-AN@CNT UTMs for most dyes was attributed to

DOI: 10.1021/acs.langmuir.6b03689
Langmuir XXXX, XXX, XXX−XXX

the better hydrophobicity of hPEA211-AN, demonstrating that hydrophobic interactions might be the primary origin of the adsorption forces, which coincides with our previously reported mechanism.[30,31]

Because of the introduction of CNTs to our hPEA adsorption systems, some dyes that once could not be adsorbed in our previous work[32] such as MB could currently be caught by the hPEA-AN@CNT UTMs. To understand whether the hPEA-AN or CNT was functioning in the adsorption process, the Q_{eq} of hPEA211-AN and CNTs was measured as a control (Figure S6). Both CNT and hPEA211-AN exhibited the ability to capture guest dye molecules, especially the maximum uptake of MB by CNTs, which explains why the UTMs could adsorb MB dyes differently than before. At the same time, CNTs were able to adsorb dyes such as EB and Cal without special selectivity, whereas our UTMs showed outstanding selectivity toward the two dyes, with the credit going to the excellent selectivity of hPEA-AN molecules. In the system of hPEA-AN@CNT UTMs, dye molecules could diffuse across the hPEA-AN network shells because the flexible hydrophilic PEO short chain could become stretched when it encountered water, allowing dye molecules through. The dye molecules could possibly be loaded both in the hPEA shell and on the surface of the CNTs. Therefore, it is the synergy of the two host materials, hPEA-AN and CNT, and not the independent action or simple superposition of the adsorption capacities that contributes to the prominent adsorption performance of hPEA-AN@CNT UTMs. More importantly, as shown in Figure 4b, the dye-removal efficiencies of hPEA-AN@CNT UTMs demonstrated selectivity as well. The removal efficiencies for several dyes were extremely high, especially for EB and ETB, up to nearly 100%, whereas for Cal, only it was lower than 20%, which provided promising feasibility for further molecular filtration and separation.

To further investigate the interaction between the adsorption capacity and the adsorption rate of hPEA-AN@CNT UTMs, time-dependent adsorption kinetics of the 12 dyes on Q_t were studied (Figure S7a,c). The comparative adsorption, namely, the ratio of the residual dye concentration to the initial concentration of 12 dyes over time, was calculated to describe the adsorption rate as well (Figure 5), using hPEA211-AN@CNT UTMs as an example. Dyes with high Q_{eq} exhibited a rapid increase in their adsorption capacity (Q_t) initially before 200 min and then continued to increase at a relatively slow rate up to 900 min, whereas the Q_t of dyes with low Q_{eq} maintained a low value and increased slowly. Similarly, a prompt decrease in comparative adsorption (C/C_0) was revealed initially, with a subsequent further gentle decrease. Moreover, after 900 min, over 90% of EB, ETB, DBF, and EVB was captured from the dye solution by the UTMs, which is in stark contrast to the ratio of only about 15% for the Cal dye. Such an adsorption rate performance was closely associated with Q_{eq}, which was independent of electrostatic interactions.

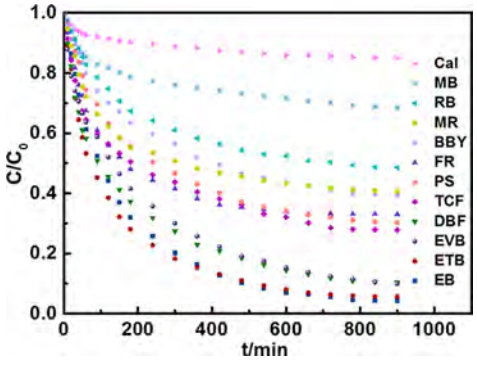

Figure 5. Time-dependent adsorption rate of hPEA211-AN@CNT UTMs for 12 different hydrophilic dyes at 25 °C (6 mL of dye solution with an initial concentration of 50 μmol/L, adsorbent 5 mg, pH = 7.2).

The adsorption kinetics of the 12 dyes accorded well with the pseudo-second-order kinetic model (see the Batch Adsorption Kinetic Studies section and Figure S7b,d), whereas the correlation coefficients, R^2, of the fitting curves were nearly 1. The apparent pseudo-second-order rate constant (k) of the seven fluorescein dyes to hPEA211-AN@CNT UTMs was carried out in comparison with that of hPEA211-AN (Figure S8 and Table S2). The rate constant k of the seven fluorescein dyes with different adsorption rates had considerable differences in magnitude, namely, the adsorption rate of EB by hPEA-AN@CNT UTMs was more than 10 times that of Cal. Moreover, compared with the hPEA-AN film itself as a reference, hPEA-AN@CNT UTMs could adsorb more dyes at a greater speed. These results demonstrated the superiority of the introduction of host CNTs to our hPEA system for increasing the uptake of more molecules, which had a dominant effect on the filtration technique over merely coating the prepared UTM materials, thus facilitating the construction of functional fibrous nanoscale networks with a more rapid penetration of water.

The thermodynamic parameters of the dye adsorption by hPEA211-AN@CNT UTMs toward ETB, Cal, BBY, and EVB, representing varied types and capacities being adsorbed, were measured to further uncover the adsorption mechanism. The thermodynamic behavior fit the Langmuir isotherm model well (see the Thermodynamic Studies of Adsorption section and Figure 6), which assumes a uniform active site energy and a monolayer adsorption mode. Furthermore, the maximum adsorption capacity at equilibrium (Q_{max}) for different dyes was found according to the Langmuir model (Table S3), manifesting that with sufficiently high initial dye concentration, UTMs could exhibit considerable promising adsorption capacities for dyes such as ETB. By contrast, thermodynamic parameters for the four dyes fitting the Freundlich model, which simulates the adsorption process with the adsorption force decreasing with site occupation, had a relatively lower correlation coefficient R^2 (Figure S9 and Table S3).

Separation of Dye Mixtures by Molecular Filtration. In real wastewater treatment systems, waste dye solutions often tend to be a mixture of dyes either of different types or with similar structures. The outstanding selective adsorption by hPEA-AN@CNT UTMs, coupled with their photo-cross-linked structure that is resistant to solvents as a result of AN photodimerization, enables further molecular filtration and separation. Breakthrough curves of ETB and Cal through hPEA211-AN@CNT UTMs (one layer) were obtained in advance by determining the flow-through outlet concentration. For ETB, which was mostly caught by the UTMs during filtration, the slightly upward trend in the breakthrough curve describing the relationship between the outlet concentration of the dye after filtration and the elution volume was revealed with an ascent that was slow initially and faster thereafter, ultimately exhibiting an S-curve. This result demonstrated that most ETB dye was absorbed at the beginning during filtration, followed by

DOI: 10.1021/acs.langmuir.6b03689
Langmuir XXXX, XXX, XXX−XXX

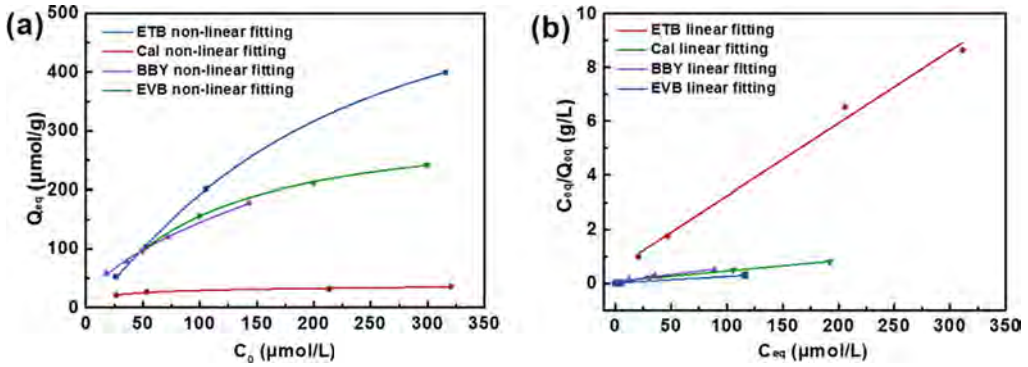

Figure 6. Adsorption isotherm fitting by the Langmuir model: adsorption of ETB, Cal, BBY, and EVB on hPEA-AN@CNT UTMs (6 mL of dye solution, pH = 7.2, 25 °C) with nonlinear fitting (a) and linear fitting (b).

a gradually diminished uptake as equilibrium was reached. On the contrary, for Cal, where nine-tenths could directly pierce through the UTMs without redundant interaction with hPEA-AN@CNTs, the outlet concentration increased quickly once the dye solution was added and reached the feed concentration rapidly. Under the experimental conditions, the final outlet concentration of the ETB dye in solution was 70% of the feed concentration when the effluent reached 90 mL using only 0.5 mg of hPEA-AN@CNT UTM as an absorbent, whereas that of the Cal dye was up to 95% of the feed concentration under the same conditions. The results were consistent with the batch-selective adsorption behaviors (Figure 7).

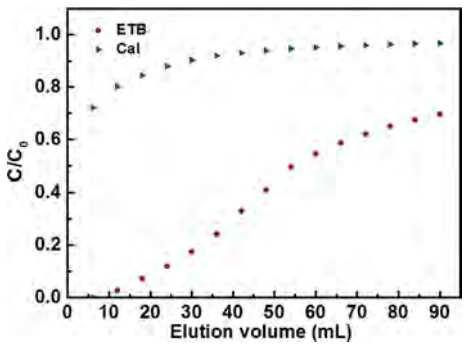

Figure 7. Breakthrough curves for ETB and Cal solutions through hPEA-AN@CNT UTMs (dye solution with the initial concentration of 10 μmol/L, adsorbent 0.5 mg, effective area of 3.14 cm^2, pH = 7.2).

Then, a mixture of dyes with similar backbones and charge states was filtered through hPEA211-AN@CNT UTMs (three layers), bearing the advantage of combining adsorption with separation. Owing to the difference in adsorptive power toward different dye molecules, the UTMs could first show selective adsorption during the filtration process. Dye molecules interacting strongly with UTMs could be captured and retained in the membranes, whereas dye molecules with weak interactions would directly flow through, for an optimum separation. Indeed, the dye molecules retained in the UTMs could be eluted, during which not only dye separation was realized but the very crucial dye recovery was also achieved.

The adsorption and filtration experiments revealed that hPEA-AN@CNT UTMs exhibited unique selective adsorption to fluorescence dyes even if they share the same backbone and are positively charged. The mixture of red ETB and yellow Cal ($[ETB]_{aq}/[Cal]_{aq}$ = 1:1), which was orange as it first passed through the UTMs, acquired a yellow filtrate after filtration (Figure 8a, left and middle). The dye concentration of the mixture before and after filtration was measured using UV−vis spectroscopy (Figure 8b). Almost all of the ETB dye was captured during the filtration process, whereas the concentration of the Cal dye stayed almost unchanged in the filtrate, and the separation efficiency was nearly 100% (by calculating the ratio of Cal concentration in solution). On the other hand, the UTMs were regenerated by flowing a NaOH solution through (mass concentration of 5‰) to remove the adsorbed dye molecules, where the absorbed ETB was removed and recovered during the desorption process to obtain a red filtrate (Figure 8a, right). The same method was implemented on the separation of an aquamarine blue mixture, which contained blue EVB and yellow Cal ($[EVB]_{aq}/[Cal]_{aq}$ = 1:1) belonging to different families. The color of the filtrate turned from blue-green to yellow for Cal (Figure 8c, left and middle), revealing that EVB molecules were adsorbed by the UTMs during the filtration process. According to the UV−vis spectra on detecting the concentration before and after filtration (Figure 8d), the concentration of EVB decreased obviously to a minimum after filtration, whereas that of Cal remained immutable, indicating a separation efficiency of up to 100%. The adsorbed EVB molecules can also be recovered from the UTMs by a NaOH solution (Figure 8c, right).

The regeneration and long-term stability of hPEA-AN@CNT UTMs are extremely significant in practice. Adsorption/desorption cycles of hPEA211-AN@CNT UTMs were implemented by successively filtrating ETB/Cal dye mixtures and a NaOH (mass concentration of 5‰) solution followed by washing with Milli-Q water. The separation efficiencies of UTMs for five cycles maintained a high level of nearly 100% with no decrease (Figure 9a), and the removal efficiencies of ETB and Cal in each cycle are summarized in Figure S10a. The UTMs still exhibited a smooth surface without obvious defects (Figure 9b,c) after cycling five times, and the cross-sectional morphology (Figure S10b) was the same as that before filtration, therefore allowing the as-prepared hPEA-AN@CNT UTMs to be an efficient and recyclable selective adsorbent for removing and recycling mixtures of different dye pollutants from water through molecular filtration.

CONCLUSIONS

We have fabricated novel hPEA-AN@CNT UTMs that possess both outstanding selectivity in the uptake of guest dye molecules and smart separation through adsorption and molecular filtration. By virtue of the π−π interactions between ANs and CNTs, well-dispersed CNTs coated with hPEA-AN

DOI: 10.1021/acs.langmuir.6b03689
Langmuir XXXX, XXX, XXX−XXX

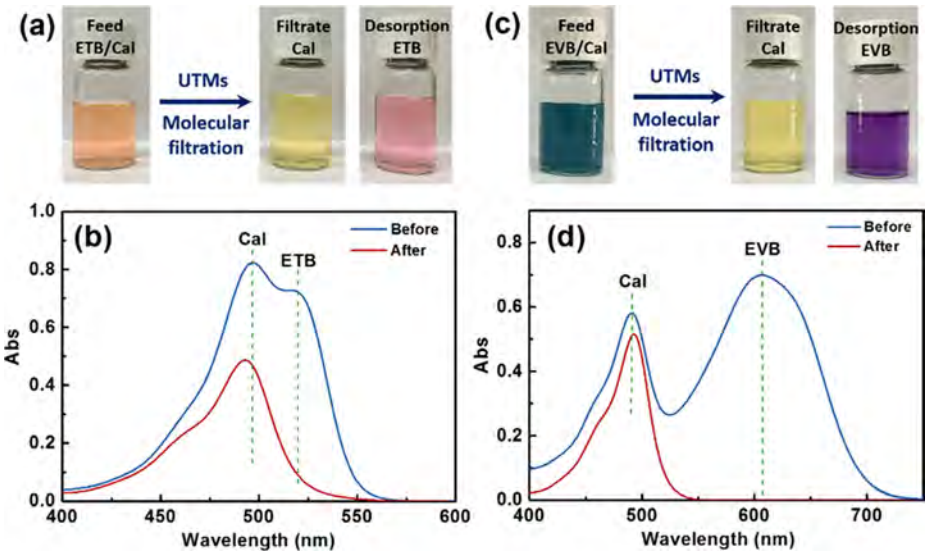

Figure 8. Separation of dyes mixtures: molecular filtration of dye mixtures of ETB/Cal (a,b) and EVB/Cal (c,d) by hPEA211-AN@CNT UTMs (15 mL of dye mixture solution, adsorbent 1.5 mg, pH = 7.2). (a,c) Photographs of ETB/Cal (a) and EVB/Cal (c) before and after filtration (the initial concentration of dyes was 10 μmol/L), as well as photographs after desorption (NaOH with a mass concentration of 5‰, 15 mL) at 25 °C; (b,d) UV−vis spectra of ETB/Cal (b) and EVB/Cal (d) mixtures before and after filtration.

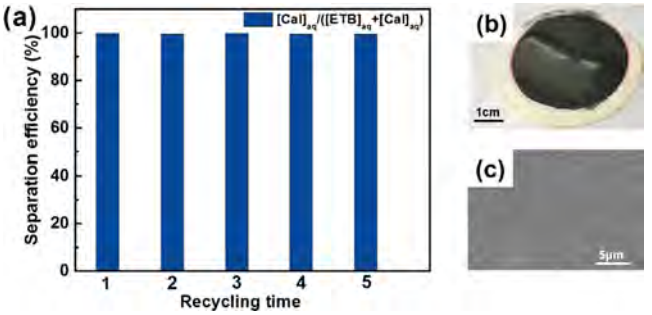

Figure 9. Regeneration of hPEA211-AN@CNT UTMs: (a) recyclability of the hPEA-AN@CNT UTMs for capturing ETB from a ETB/Cal mixture solution; (b) photograph of the UTM after cycling five times; (c) SEM image of a UTM section after cycling five times.

could form three-dimensional nanoscale network-structured UTMs via a specific but simple vacuum-assisted filtration preparation technique, which could be further cross-linked through photoinduced dimerization of AN molecules, stabilizing the UTMs toward solvents. The obtained hPEA-AN@CNT UTMs facilitated not only selective absorption with a high efficiency but also the separation and recycling of dyes mixtures even with similar backbones and charge states during the process of molecular filtration. It is the synergy and efficiencies of host hPEA-AN molecules and CNTs and the fibrous network structure of the UTMs that contribute to the superior adsorption performance of hPEA-AN@CNT UTMs, which could concurrently be regenerated without efficiency loss. These novel features make the hPEA-AN@CNT UTMs a potential candidate for use in wastewater treatment, especially for the removal and simultaneous separation of hydrophilic dyes with similar properties.

METHODS

Materials. hPEA-AN was synthesized according to the previous work of our group.[55] Multiwalled CNTs were purchased from Alpha Nano Technology Co., Ltd (Chengdu, China) and were used without further purification.

Preparation and Fabrication of hPEA-AN@CNT UTMs. CNTs (60 mg) and hPEA-AN (90 mg) were added to 60 mL of Milli-Q water; then, the mixture was ultrasonically dispersed (ShuMei KQ218 models, 40 kHz, 100 W, Kunshan Ultrasonic Instrument Co., Ltd) for 3 h, followed by further fast stirring for 24 h. After left for 2 h, the supernatant was successively subjected to low-speed centrifugation pretreatment (Xiang Yi, China) at 500 rpm for 5 min and high-speed centrifugation at 9000 rpm for 10 min to obtain hPEA-AN@CNT composite dispersions. hPEA-AN@CNT UTMs were fabricated using the vacuum-assisted sand core filtration process, namely, the addition of 10 or 60 mL of the above-mentioned hPEA-AN@CNT composite dispersion upon cellulose membranes to produce membranes of different thicknesses and then drying at 40 °C for 6 h, followed by further cross-linking through the photodimerization of anthracene for 30 min using 365 nm UV LED lamp (Uvata, China) with an intensity of about 8.4 mW/cm^2.

Batch Adsorption of the 12 Hydrophilic Dyes. Twelve different hydrophilic dyes, as illustrated in Scheme 2, were chosen to study the adsorption behavior of the hPEA-AN@CNT membrane at 25 °C. In the batch adsorption capacity test, the initial concentration of all dyes in 6 mL of phosphate-buffered aqueous media at pH 7.2 was 300 μmol/L, which was measured from the calibration curves of dyes, except for those dyes with low solubility that cannot be dissolved at such a high concentration in the phosphate buffer: BBY (200 μmol/L), PS (100 μmol/L), MR (100 μmol/L); 5 mg of three kinds of dried adsorbents (hPEA-AN@CNT, hPEA-AN, CNT) was added, and adsorption capacity tests were carried out after 48 h.

The amount of adsorption of dyes per gram of adsorbent at time t, Q_t (μmol/g), is defined as follows

$$Q_t = \frac{(C_0 - C_t)}{M} V \tag{1}$$

where C_0 (μmol/L) is the initial concentration of dyes in the solution, C_t (μmol/L) is the concentration of dyes at time t (min), V (L) is the volume of the solution, and M (g) is the mass of the adsorbent being used. When adsorption reached equilibrium ($C_t = C_{eq}$), $Q_t = Q_{eq}$, in which Q_{eq} (μmol/g) is defined as the amount of dyes adsorbed per gram of adsorbent at equilibrium.

The efficiency of dye removal by the hPEA-AN@CNT UTMs was determined by the following equation[14]

$$\text{Dye removal efficiency} = \frac{C_0 - C_t}{c_0} \times 100\% \tag{2}$$

DOI: 10.1021/acs.langmuir.6b03689
Langmuir XXXX, XXX, XXX−XXX

where C_0 and C_t (μmol/L) are the initial and residual concentrations of dye before and after adsorption, respectively.

Batch Adsorption Kinetic Studies. In the batch adsorption kinetic experiment, the initial concentration of all dyes was 50 μmol/L, whereas the other conditions were the same. The uptake rate of each adsorbent was best described by Ho and McKay's pseudo-second-order adsorption model,[14] which was generated by plotting t/Q_t to t, and the common linearized form is shown as follows

$$\frac{t}{Q_t} = \frac{t}{Q_{eq}} + \frac{1}{kQ_{eq}^2} \quad (3)$$

where Q_t and Q_{eq} (μmol/g) are the absorbate uptakes at time t (min) and at equilibrium, respectively, and k (g·μmol^{-1}·min^{-1}) is the second-order rate constant.

Thermodynamic Studies of Adsorption. A Langmuir adsorption isotherm[64] was generated by plotting C_{eq}/Q_{eq} versus C_{eq} in the following equation

$$\frac{C_{eq}}{Q_{eq}} = \frac{C_{eq}}{Q_{max}} + \frac{1}{K_L Q_{max}} \quad (4)$$

where Q_{eq} (μmol/g) is the amount of adsorbed dyes per gram of adsorbent at equilibrium, Q_{max} (μmol/g) is the maximum adsorption capacity of the adsorbent at equilibrium, C_{eq} (μmol/L) is the equilibrium concentration of dyes, and K_L (L/μmol) is the Langmuir adsorption constant.

A Freundlich adsorption isotherm[65] was generated by plotting ln Q_{eq} to ln C_0 in the equation as follows

$$\ln Q_{eq} = \ln K_F + b_F \ln C_{eq} \quad (5)$$

where Q_{eq} (μmol/g) is the amount of adsorbed dyes per gram of the adsorbent at equilibrium, C_{eq} (μmol/L) is the equilibrium concentration of dyes, and K_F is the Freundlich constant, and b_F is a constant for depicting the adsorption intensity.

Molecular Filtration Performance of hPEA-AN@CNT UTMs. The membrane filtration experiments were conducted on 0.5 mg UTMs with an effective area of 3.14 cm^2; dye solutions with an initial concentration of 10 μmol/L were forced to filter through the film. In the membrane filtration−separation experiment and adsorption/desorption cycling, three pieces of 0.5 mg UTMs were stacked up to separate 15 mL of mixed dyes with the initial concentration of 10 μmol/L. A NaOH solution (15 mL; mass concentration of 5‰) and 15 mL of Milli-Q water were added in succession before the next cycle.

Characterizations. *TEM.* TEM morphologies of CNT and hPEA-AN@CNT dispersions were recorded on a JEM-2100 (JEOL Ltd, Japan) transmission electron microscope operated at an acceleration voltage of 200 kV. Each sample was dropped onto a Lacey support grid and dried at 25 °C for 48 h. No staining treatment was performed for the measurement.

SEM. A JSM-7401F (JEOL Ltd., Japan) field-emission scanning electron microscope (FE-SEM) operated at an acceleration voltage of 5 kV was used to observe the surface and section morphologies of hPEA-AN@CNT membranes. For section samples, low-temperature brittle fracture was carried out. Before getting the images, the samples were sputter-coated with gold to minimize charging.

LSCM. The fluorescence image of hPEA-AN@CNT was viewed using a TCS SP8 STED 3X LSCM (Leica, Germany) equipped with UV lasers. The sample was prepared by dropping the hPEA-AN@CNT dispersions onto a coverslip and then dried at 25 °C for 48 h.

UV−Vis Spectroscopy. A TU-1901 UV−vis spectroscope (Persee, China) was used to measure the absorbance of different dyes before and after adsorption as well as the process of anthracene photocross-linking.

Fluorescence Spectroscopy and Fluorescence Decay. The fluorescence spectra were recorded to monitor the behavior of anthracene via an LS-55B fluorescence meter (Perkin-Elmer, Inc., USA) with the excitation wavelength at 370 nm. The fluorescence decay of hPEA-AN and hPEA-AN@CNT was recorded using the same instrument. The excitation wavelength was 370 nm, and the emission wavelength was 430 nm to minimize the interference. All solutions were equilibrated for 10 min before measurement.

Raman Microscope. The interaction between anthracene and CNTs was probed using a DXR Raman microscope (Thermo Fisher Scientific, USA) at an excitation wavelength of 532 nm.

TGA. TGA (Perkin-Elmer, Inc., USA) was used to measure the content of hPEA-AN in the hPEA-AN@CNT composites at a heating rate of 20 °C/min from room temperature to 600 °C under a flowing N_2 atmosphere.

XPS. XPS was carried out using an Axis Ultra DLD X-ray photoelectron spectrometer (Kratos, Japan) to analyze the content of elements C, O, and N in CNTs and hPEA-AN@CNTs.

■ ASSOCIATED CONTENT

Supporting Information

The Supporting Information is available free of charge on the ACS Publications website at DOI: 10.1021/acs.langmuir.6b03689.

Photographs of dispersions of CNT, hPEA@CNT, and hPEA-AN@CNT; TEM image of CNT; UV−vis spectra steady-state fluorescence spectra of hPEA-AN and hPEA-AN@CNT; TGA data of CNT, hPEA-AN, hPEA-AN@CNT and the calculation of coating rate; photograph and SEM images of hPEA101-AN@CNT UTMs; photo-cross-linking of anthracene measured using UV−vis spectra; equilibrium adsorption capacities of CNT and hPEA211-AN; adsorption capacity Q_t versus time for the adsorption of dyes and kinetic parameters onto hPEA211-AN@CNT UTMs and hPEA211-AN membranes; adsorption isotherms fitting using Freundlich model; removal efficiency during the separation of hPEA211-AN@CNT UTMs; and SEM image of the hPEA211-AN@CNT UTM section after cycling (PDF)

■ AUTHOR INFORMATION

Corresponding Author

*E-mail: ponygle@sjtu.edu.cn.

ORCID

Xuesong Jiang: 0000-0002-8976-8491

Notes

The authors declare no competing financial interest.

■ ACKNOWLEDGMENTS

The authors thank the National Basic Research Program (2013CB834506), the National Natural Science Foundation of China (21274088, 51373098, and 21522403), and the Education Commission of Shanghai Municipal Government (15SG13) for their financial support.

■ REFERENCES

(1) Shannon, M. A.; Bohn, P. W.; Elimelech, M.; Georgiadis, J. G.; Mariñas, B. J.; Mayes, A. M. Science and Technology for Water Purification in the Coming Decades. *Nature* **2008**, *452*, 301−310.

(2) Banat, I. M.; Nigam, P.; Singh, D.; Marchant, R. Microbial Decolorization of Textile-Dyecontaining Effluents: A Review. *Bioresour. Technol.* **1996**, *58*, 217−227.

(3) Liu, F.; Chung, S.; Oh, G.; Seo, T. S. Three-Dimensional Graphene Oxide Nanostructure for Fast and Efficient Water-Soluble Dye Removal. *ACS Appl. Mater. Interfaces* **2012**, *4*, 922−927.

(4) Chethana, M.; Sorokhaibam, L. G.; Bhandari, V. M.; Raja, S.; Ranade, V. V. Green Approach to Dye Wastewater Treatment Using Biocoagulants. *ACS Sustainable Chem. Eng.* **2016**, *4*, 2495−2507.

(5) Amaral, F. M.; Kato, M. T.; Florêncio, L.; Gavazza, S. Color, Organic Matter and Sulfate Removal from Textile Effluents by

DOI: 10.1021/acs.langmuir.6b03689
Langmuir XXXX, XXX, XXX−XXX

Anaerobic and Aerobic Processes. *Bioresour. Technol.* **2014**, *163*, 364−369.
(6) Liu, L.; Gao, Z. Y.; Su, X. P.; Chen, X.; Jiang, L.; Yao, J. M. Adsorption Removal of Dyes from Single and Binary Solutions Using a Cellulose-Based Bioadsorbent. *ACS Sustainable Chem. Eng.* **2015**, *3*, 432−442.
(7) Li, C.; Zhuang, Z.; Huang, F.; Wu, Z.; Hong, Y.; Lin, Z. Recycling Rare Earth Elements from Industrial Wastewater with Flowerlike Nano-Mg(OH)$_2$. *ACS Appl. Mater. Interfaces* **2013**, *5*, 9719−9725.
(8) Li, B.; Dong, Y.; Zou, C.; Xu, Y. Iron(III)-Alginate Fiber Complex as a Highly Effective and Stable Heterogeneous Fenton Photocatalyst for Mineralization of Organic Dye. *Ind. Eng. Chem. Res.* **2014**, *53*, 4199−4206.
(9) Oladoja, N. A.; Raji, I. O.; Olaseni, S. E.; Onimisi, T. D. In Situ Hybridization of Waste Dyes into Growing Particles of Calcium Derivatives Synthesized from a Gastropod Shell (Achatina Achatina). *Chem. Eng. J.* **2011**, *171*, 941−950.
(10) Ahmad, A.; Mohd-Setapar, S. H.; Chuong, C. S.; Khatoon, A.; Wani, W. A.; Kumar, R.; Rafatullah, M. Recent Advances in New Generation Dye Removal Technologies: Novel Search for Approaches to Reprocess Wastewater. *RSC Adv.* **2015**, *5*, 30801−30818.
(11) Taştan, B. E.; Karatay, S. E.; Dönmez, G. Bioremoval of Textile Dyes with Different Chemical Structures by Aspergillus Versicolor in Molasses Medium. *Water Sci. Technol.* **2012**, *66*, 2177−2184.
(12) Crini, G. Non-Conventional Low-Cost Adsorbents for Dye Removal: A Review. *Bioresour. Technol.* **2006**, *97*, 1061−1085.
(13) Qiu, W.-Z.; Yang, H.-C.; Wan, L.-S.; Xu, Z.-K. Co-Deposition of Catechol/Polyethyleneimine on Porous Membranes for Efficient Decolorization of Dye Water. *J. Mater. Chem. A* **2015**, *3*, 14438−14444.
(14) Alsbaiee, A.; Smith, B. J.; Xiao, L.; Ling, Y.; Helbling, D. E.; Dichtel, W. R. Rapid Removal of Organic Micropollutants from Water by a Porous β-Cyclodextrin Polymer. *Nature* **2016**, *529*, 190−194.
(15) Putra, E. K.; Pranowo, R.; Sunarso, J.; Indraswati, N.; Ismadji, S. Performance of Activated Carbon and Bentonite for Adsorption of Amoxicillin from Wastewater: Mechanisms, Isotherms and Kinetics. *Water Res.* **2009**, *43*, 2419−2430.
(16) Ferrero, F.; Periolatto, M. Functionalized Fibrous Materials for the Removal of Dyes. *Clean Technol. Environ. Policy* **2011**, *14*, 487−494.
(17) Chen, Y.; Chen, L.; Bai, H.; Li, L. Graphene Oxide−Chitosan Composite Hydrogels as Broad-Spectrum Adsorbents for Water Purification. *J. Mater. Chem. A* **2013**, *1*, 1992−2001.
(18) Wang, N.; Zhou, L.; Guo, J.; Ye, Q.; Lin, J.-M.; Yuan, J. Adsorption of Environmental Pollutants Using Magnetic Hybrid Nanoparticles Modified with β-Cyclodextrin. *Appl. Surf. Sci.* **2014**, *305*, 267−273.
(19) Zhao, R.; Wang, Y.; Li, X.; Sun, B.; Wang, C. Synthesis of Beta-Cyclodextrin-Based Electrospun Nanofiber Membranes for Highly Efficient Adsorption and Separation of Methylene Blue. *ACS Appl. Mater. Interfaces* **2015**, *7*, 26649−26657.
(20) van Kuringen, H. P. C.; Eikelboom, G. M.; Shishmanova, I. K.; Broer, D. J.; Schenning, A. P. H. J. Responsive Nanoporous Smectic Liquid Crystal Polymer Networks as Efficient and Selective Adsorbents. *Adv. Funct. Mater.* **2014**, *24*, 5045−5051.
(21) Molina, E. F.; Parreira, R. L. T.; De Faria, E. H.; de Carvalho, H. W. P.; Caramori, G. F.; Coimbra, D. F.; Nassar, E. J.; Ciuffi, K. J. Ureasil-Poly(ethylene oxide) Hybrid Matrix for Selective Adsorption and Separation of Dyes from Water. *Langmuir* **2014**, *30*, 3857−3868.
(22) Wan, D.; Jin, M.; Pu, H. Charge-Selective Separation and Recovery of Organic Ions by Polymeric Micelles. *J. Polym. Sci., Part B: Polym. Phys.* **2014**, *52*, 872−881.
(23) Moura, A. L. A.; de Oliveira, L. K.; Ciuffi, K. J.; Molina, E. F. Influence of the Hydrophilic/Hydrophobic Nature of Polyetheramines on the Interaction between Amine−Alcohol−Silicate Hybrids and Anionic Dyes for Effective Water Cleaning. *J. Mater. Chem. A* **2015**, *3*, 16020−16032.
(24) van Kuringen, H. P. C.; Leijten, Z. J. W. A.; Gelebart, A. H.; Mulder, D. J.; Portale, G.; Broer, D. J.; Schenning, A. P. H. J. Photoresponsive Nanoporous Smectic Liquid Crystalline Polymer Networks: Changing the Number of Binding Sites and Pore Dimensions in Polymer Adsorbents by Light. *Macromolecules* **2015**, *48*, 4073−4080.
(25) Wei, W.; Lu, R.; Xie, H.; Zhang, Y.; Bai, X.; Gu, L.; Da, R.; Liu, X. Selective Adsorption and Separation of Dyes from an Aqueous Solution on Organic−Inorganic Hybrid Cyclomatrix Polyphosphazene Submicro-Spheres. *J. Mater. Chem. A* **2015**, *3*, 4314−4322.
(26) Qin, Y.; Wang, L.; Zhao, C.; Chen, D.; Ma, Y.; Yang, W. Ammonium-Functionalized Hollow Polymer Particles as a pH-Responsive Adsorbent for Selective Removal of Acid Dye. *ACS Appl. Mater. Interfaces* **2016**, *8*, 16690−16698.
(27) Karan, C. K.; Bhattacharjee, M. Self-Healing and Moldable Metallogels as the Recyclable Materials for Selective Dye Adsorption and Separation. *ACS Appl. Mater. Interfaces* **2016**, *8*, 5526−5535.
(28) Deng, S.; Wang, R.; Xu, H.; Jiang, X.; Yin, J. Hybrid Hydrogels of Hyperbranched Poly(ether amine)s (hPEAs) for Selective Adsorption of Guest Molecules and Separation of Dyes. *J. Mater. Chem.* **2012**, *22*, 10055−10061.
(29) Wang, R.; Yu, B.; Jiang, X.; Yin, J. Understanding the Host-Guest Interaction between Responsive Core-Crosslinked Hybrid Nanoparticles of Hyperbranched Poly(ether amine) and Dyes: The Selective Adsorption and Smart Separation of Dyes in Water. *Adv. Funct. Mater.* **2012**, *22*, 2606−2616.
(30) Deng, S.; Xu, H.; Jiang, X.; Yin, J. Poly(vinyl alcohol) (PVA)-Enhanced Hybrid Hydrogels of Hyperbranched Poly(ether amine) (hPEA) for Selective Adsorption and Separation of Dyes. *Macromolecules* **2013**, *46*, 2399−2406.
(31) Zhang, P.; Yin, J.; Jiang, X. Hyperbranched Poly(ether amine) (hPEA)/Poly(vinyl alcohol) (PVA) Interpenetrating Network (IPN) for Selective Adsorption and Separation of Guest Homologues. *Langmuir* **2014**, *30*, 14597−14605.
(32) Li, J.; Su, Z.; Xu, H.; Ma, X.; Yin, J.; Jiang, X. Supramolecular Networks of Hyperbranched Poly(ether amine) (hPEA) Nanogel/Chitosan (CS) for the Selective Adsorption and Separation of Guest Molecules. *Macromolecules* **2015**, *48*, 2022−2029.
(33) Fu, G.; Su, Z.; Jiang, X.; Yin, J. Photo-Crosslinked Nanofibers of Poly(ether amine) (PEA) for the Ultrafast Separation of Dyes through Molecular Filtration. *Polym. Chem.* **2014**, *5*, 2027−2034.
(34) Yuan, J.; Liu, X.; Akbulut, O.; Hu, J.; Suib, S. L.; Kong, J.; Stellacci, F. Superwetting Nanowire Membranes for Selective Absorption. *Nat. Nanotechnol.* **2008**, *3*, 332−336.
(35) Geise, G. M.; Lee, H.-S.; Miller, D. J.; Freeman, B. D.; McGrath, J. E.; Paul, D. R. Water Purification by Membranes: The Role of Polymer Science. *J. Polym. Sci., Part B: Polym. Phys.* **2010**, *48*, 1685−1718.
(36) Liang, H.-W.; Wang, L.; Chen, P.-Y.; Lin, H.-T.; Chen, L.-F.; He, D.; Yu, S.-H. Carbonaceous Nanofiber Membranes for Selective Filtration and Separation of Nanoparticles. *Adv. Mater.* **2010**, *22*, 4691−4695.
(37) Zheng, Y.; Yao, G.; Cheng, Q.; Yu, S.; Liu, M.; Gao, C. Positively Charged Thin-Film Composite Hollow Fiber Nanofiltration Membrane for the Removal of Cationic Dyes through Submerged Filtration. *Desalination* **2013**, *328*, 42−50.
(38) Chen, P.; Liang, H.-W.; Lv, X.-H.; Zhu, H.-Z.; Yao, H.-B.; Yu, S.-H. Carbonaceous Nanofiber Membrane Functionalized by Beta-Cyclodextrins for Molecular Filtration. *ACS Nano* **2011**, *5*, 5928−5935.
(39) Liang, H.-W.; Cao, X.; Zhang, W.-J.; Lin, H.-T.; Zhou, F.; Chen, L.-F.; Yu, S.-H. Robust and Highly Efficient Free-Standing Carbonaceous Nanofiber Membranes for Water Purification. *Adv. Funct. Mater.* **2011**, *21*, 3851−3858.
(40) Liu, Z.; Yi, Y.; Gauczinski, J.; Xu, H.; Schönhoff, M.; Zhang, X. Surface Molecular Imprinted Layer-by-Layer Film Attached to a Porous Membrane for Selective Filtration. *Langmuir* **2011**, *27*, 11806−11812.
(41) Li, G.; Zhu, Z.; Qi, B.; Liu, G.; Wu, P.; Zeng, G.; Zhang, Y.; Wang, W.; Sun, Y. Rapid Capture of Ponceau S Via a Hierarchical

DOI: 10.1021/acs.langmuir.6b03689
Langmuir XXXX, XXX, XXX−XXX

Organic−Inorganic Hybrid Nanofibrous Membrane. *J. Mater. Chem. A* **2016**, *4*, 5423−5427.
(42) Baughman, R. H.; Zakhidov, A. A.; de Heer, W. A. Carbon Nanotubes—the Route toward Applications. *Science* **2002**, *297*, 787−792.
(43) Lu, W.; Zu, M.; Byun, J. H.; Kim, B.-S.; Chou, T.-W. State of the Art of Carbon Nanotube Fibers: Opportunities and Challenges. *Adv. Mater.* **2012**, *24*, 1805−1833.
(44) Cummings, A. In *Nanotechnology 2008: Materials, Fabrication, Particles, and Characterization*; Laudon, M., Romanowicz, B., Eds; CRC Press: Florida, 2008; pp 175−178.
(45) De Volder, M. F.; Tawfick, S. H.; Baughman, R. H.; Hart, A. J. Carbon Nanotubes: Present and Future Commercial Applications. *Science* **2013**, *339*, 535−539.
(46) Zhao, Y.; Abdullayev, E.; Vasiliev, A.; Lvov, Y. Halloysite Nanotubule Clay for Efficient Water Purification. *J. Colloid Interface Sci.* **2013**, *406*, 121−129.
(47) Zhao, Y.; Abdullayev, E.; Lvov, Y. Nanotubular Halloysite Clay as Efficient Water Filtration System for Removal of Cationic and Anionic Dyes. *IOP Conf. Ser.: Mater. Sci. Eng.* **2014**, *64*, 012043.
(48) Chen, X.; Hong, L.; Xu, Y.; Ong, Z. W. Ceramic Pore Channels with Inducted Carbon Nanotubes for Removing Oil from Water. *ACS Appl. Mater. Interfaces* **2012**, *4*, 1909−1918.
(49) Hu, L.; Gao, S.; Ding, X.; Wang, D.; Jiang, J.; Jin, J.; Jiang, L. Photothermal-Responsive Single-Walled Carbon Nanotube-Based Ultrathin Membranes for On/Off Switchable Separation of Oil-in-Water Nanoemulsions. *ACS Nano* **2015**, *9*, 4835−4842.
(50) Jie, G.; Kongyin, Z.; Xinxin, Z.; Zhijiang, C.; Min, C.; Tian, C.; Junfu, W. Preparation and Characterization of Carboxyl Multi-Walled Carbon Nanotubes/Calcium Alginate Composite Hydrogel Nano-Filtration Membrane. *Mater. Lett.* **2015**, *157*, 112−115.
(51) Zhao, F.-Y.; Ji, Y.-L.; Weng, X.-D.; Mi, Y.-F.; Ye, C.-C.; An, Q.-F.; Gao, C.-J. High-Flux Positively Charged Nanocomposite Nanofiltration Membranes Filled with Poly(dopamine) Modified Multiwall Carbon Nanotubes. *ACS Appl. Mater. Interfaces* **2016**, *8*, 6693−6700.
(52) Vecitis, C. D.; Gao, G.; Liu, H. Electrochemical Carbon Nanotube Filter for Adsorption, Desorption, and Oxidation of Aqueous Dyes and Anions. *J. Phys. Chem. C* **2011**, *115*, 3621−3629.
(53) Guo, J.; Zhang, Q.; Cai, Z.; Zhao, K. Preparation and Dye Filtration Property of Electrospun Polyhydroxybutyrate-Calcium Alginate/Carbon Nanotubes Composite Nanofibrous Filtration Membrane. *Sep. Purif. Technol.* **2016**, *161*, 69−79.
(54) Loginov, M.; Lebovka, N.; Vorobiev, E. Hybrid Multiwalled Carbon Nanotube−Laponite Sorbent for Removal of Methylene Blue from Aqueous Solutions. *J. Colloid Interface Sci.* **2014**, *431*, 241−249.
(55) Yu, B.; Jiang, X.; Yin, J. Responsive Fluorescent Core-Crosslinked Polymer Particles Based on the Anthracene-Containing Hyperbranched Poly(ether amine) (hPEA−AN). *Soft Matter* **2011**, *7*, 6853.
(56) Byrne, M. T.; Gun'ko, Y. K. Recent Advances in Research on Carbon Nanotube-Polymer Composites. *Adv. Mater.* **2010**, *22*, 1672−1688.
(57) Yu, G.; Xue, M.; Zhang, Z.; Li, J.; Han, C.; Huang, F. A Water-Soluble Pillar[6]arene: Synthesis, Host−Guest Chemistry, and Its Application in Dispersion of Multiwalled Carbon Nanotubes in Water. *J. Am. Chem. Soc.* **2012**, *134*, 13248−13251.
(58) Ding, Y.; Chen, S.; Xu, H.; Wang, Z.; Zhang, X.; Ngo, T. H.; Smet, M. Reversible Dispersion of Single-Walled Carbon Nanotubes Based on a CO_2-Responsive Dispersant. *Langmuir* **2010**, *26*, 16667−16671.
(59) Chen, S.; Jiang, Y.; Wang, Z.; Zhang, X.; Dai, L.; Smet, M. Light-Controlled Single-Walled Carbon Nanotube Dispersions in Aqueous Solution. *Langmuir* **2008**, *24*, 9233−9236.
(60) Yu, B.; Jiang, X.; Yin, G.; Yin, J. Multistimuli-Responsive Hyperbranched Poly(ether amine)s. *J. Polym. Sci., Part A: Polym. Chem.* **2010**, *48*, 4252−4261.
(61) Sun, P.; Wang, K.; Zhu, H. Recent Developments in Graphene-Based Membranes: Structure, Mass-Transport Mechanism and Potential Applications. *Adv. Mater.* **2016**, *28*, 2287−2310.
(62) Su, Z.; Yu, B.; Jiang, X.; Yin, J. Responsive Fluorescent Nanorods from Coassembly of Fullerene (C_{60}) and Anthracene-Ended Hyperbranched Poly(ether amine) (AN-hPEA). *Macromolecules* **2013**, *46*, 3699−3707.
(63) Pandey, A.; Singh, P.; Iyengar, L. Bacterial Decolorization and Degradation of Azo Dyes. *Int. Biodeterior. Biodegrad.* **2007**, *59*, 73−84.
(64) Mittal, A.; Kurup, L.; Mittal, J. Freundlich and Langmuir Adsorption Isotherms and Kinetics for the Removal of Tartrazine from Aqueous Solutions Using Hen Feathers. *J. Hazard. Mater.* **2007**, *146*, 243−248.
(65) García-Zubiri, I. X.; González-Gaitano, G.; Isasi, J. R. Sorption Models in Cyclodextrin Polymers: Langmuir, Freundlich, and a Dual-Mode Approach. *J. Colloid Interface Sci.* **2009**, *337*, 11−18.

DOI: 10.1021/acs.langmuir.6b03689
Langmuir XXXX, XXX, XXX−XXX